Nonlinear stability of wall-bounded flows using the One-Way Navier-Stokes (OWNS) Equations

Michael K. Sleeman* and Tim Colonius†
California Institute of Technology, Pasadena, CA, USA

Matthew T. Lakebrink‡
Boeing Research & Technology, Hazelwood, MO, 63042, United States

We extend the One-Way Navier Stokes (OWNS) approach to support nonlinear interactions between waves of different frequencies, which will enable nonlinear analysis of instability and transition. In linear OWNS, the linearized Navier-Stokes equations are modified such that upstream propagating modes are removed, so that they can be solved efficiently in the frequency domain as a spatial initial-value (marching) problem. Linear OWNS confers numerous advantages over the parabolized stability equations (PSE) that we seek to extend to nonlinear analysis. In the proposed method, the fully nonlinear Navier-Stokes equations are marched in the downstream direction. At each step of the march, the projection operator from the linear OWNS procedure is applied to (approximately) remove modes with upstream group velocity. We validate the method by examining the nonlinear evolution of two- and three-dimensional disturbances in a low-speed Blasius boundary layer by comparing with PSE and DNS results from the literature.

I. Introduction

Hydrodynamic stability analysis is a critical tool for predicting laminar-turbulent transition in boundary layer flows. Modern industry tools use linear theory to predict transition onset, often using either the e^N-method [1, 2] or the variable N-factor approach [3] to extrapolate through nonlinear transition. Fundamentally, transition can be studied using direct numerical simulation (DNS) [4–6], but this approach is limited by its large computational cost. The nonlinear parabolized stability equations (PSE) entail a much lower computational cost [7], but convergence issues limit its use to the early stages of transition [8, 9]. Even in the linear case, however, PSE is unable to (accurately) track non-modal and multi-modal instabilities [9], and its minimum step size for stability prevents capturing all length scales in the streamwise direction, which is particularly problematic when extending to the nonlinear regime.

Linear OWNS overcomes these limitations of linear PSE, but at a greater computational cost. The OWNS approach does not have a minimum step size for stability, which means that arbitrarily small steps can be taken to resolve all of the length scales, enabling OWNS to capture non-modal and multi-modal interactions. The linear OWNS approach has previously been applied to two-dimensional (2D) and three-dimensional (3D) boundary-layer flows [10]. In particular, linear OWNS approach has proven useful for hypersonic boundary layer flows [11–13] where classical stability analysis methods often fail. Previous work on linear OWNS has demonstrated its robustness, which makes it well-suited to nonlinear stability analysis.

In this paper, we extend the OWNS methodology to support nonlinear interactions between waves of different frequencies and spanwise wavenumbers. In section II we present the governing equations and details of the method. In section III, we demonstrate and validate the nonlinear OWNS approach for 2D and 3D boundary-layer flows. Finally, in section IV we present plans for future work.

*PhD Candidate, Mechanical and Civil Engineering.
†Frank and Ora Lee Marble Professor of Mechanical and Medical Engineering.
‡Boeing Associated Technical Fellow.

II. Method

The compressible Navier-Stokes equations are written in Cartesian coordinates in terms of the specific volume ν, velocity $\boldsymbol{u} = (u, v, w)$, and pressure p:

$$\frac{D\nu}{Dt} - \nu(\nabla \cdot \boldsymbol{u}) = 0, \tag{1a}$$

$$\frac{D\boldsymbol{u}}{Dt} + \nu\nabla p = \frac{1}{Re}\nu\nabla^2\boldsymbol{u}, \tag{1b}$$

$$\frac{Dp}{Dt} + \gamma p(\nabla \cdot \boldsymbol{u}) = \frac{\gamma}{PrRe}(\nu\nabla^2 p + p\nabla^2\nu). \tag{1c}$$

We have non-dimensionalized the equations using the free-stream speed of sound (c_∞), the free-stream specific volume (ν_∞), the Blasius length scale ($\delta_0 = \sqrt{\frac{x_0\nu_\infty}{c_\infty}}$), and the free-stream fluid properties. This study focuses on low-speed boundary layer flows, so we approximate the fluid as a perfect gas with constant fluid properties.

We define a vector of flow quantities $\boldsymbol{q} = (\nu, u, v, w, p)$ and write the equations in operator form as

$$\frac{\partial \boldsymbol{q}}{\partial t} + \mathcal{N}(\boldsymbol{q}, \boldsymbol{q}) = 0. \tag{2}$$

where $\mathcal{N}$ is a bilinear operator

$$\mathcal{N}(\boldsymbol{q}, \boldsymbol{q}) = A(\boldsymbol{q})\frac{\partial \boldsymbol{q}}{\partial x} + B_y(\boldsymbol{q})\frac{\partial \boldsymbol{q}}{\partial y} + B_z(\boldsymbol{q})\frac{\partial \boldsymbol{q}}{\partial z} + B_2(\boldsymbol{q})\Big(\frac{\partial^2 \boldsymbol{q}}{\partial x^2} + \frac{\partial^2 \boldsymbol{q}}{\partial y^2} + \frac{\partial^2 \boldsymbol{q}}{\partial z^2}\Big), \tag{3}$$

where the A and B operators are defined in appendix IV.A. Here, x, y, z, correspond to the streamwise, transverse and spanwise directions, respectively.

We introduce the Reynolds decomposition

$$\boldsymbol{q}(x, y, z, t) = \bar{\boldsymbol{q}}(x, y, z) + \boldsymbol{q}'(x, y, z, t) \tag{4}$$

where $\bar{\boldsymbol{q}}$ is a time-invariant equilibrium solution so that $\mathcal{N}(\bar{\boldsymbol{q}}, \bar{\boldsymbol{q}}) = 0$. The nonlinear disturbance equations are

$$\frac{\partial \boldsymbol{q}'}{\partial t} + \mathcal{N}(\bar{\boldsymbol{q}}, \boldsymbol{q}') + \mathcal{N}(\boldsymbol{q}', \bar{\boldsymbol{q}}) = -\mathcal{N}(\boldsymbol{q}', \boldsymbol{q}'), \tag{5}$$

where the nonlinear terms are on the right-hand side.

Previous work on linear OWNS has often neglected the second streamwise derivatives of the disturbance variable (i.e., $\partial^2\boldsymbol{q}'/\partial x^2$) because this simplifies the spatial-marching procedure without significantly impacting the accuracy of the solution [10, 11, 14]. Neglecting this term also greatly simplifies the exposition of the nonlinear OWNS procedure. However, we have found that this term impacts significantly the accuracy of the nonlinear calculation, so we will first neglect it to explain how the nonlinear OWNS procedure works, and then re-introduce it in an approximate way to perform our stability calculations.

A. Semi-discrete stability equations

The OWNS procedure is applied to the semi-discrete stability equations, so we start by discretizing in the wall-normal direction using a fourth-order central finite difference scheme. We define the linear operator $C(\bar{\boldsymbol{q}})$ such that

$$C(\bar{\boldsymbol{q}})\boldsymbol{q}' = \mathcal{N}(\boldsymbol{q}', \bar{\boldsymbol{q}}), \tag{6}$$

and then introduce the differentiation matrix D where $\partial\boldsymbol{q}/\partial y \approx D\boldsymbol{q}$ and $\partial^2\boldsymbol{q}/\partial y^2 \approx D^2\boldsymbol{q}$, which is used to further define the linear operator $L(\bar{\boldsymbol{q}})$ such that

$$L(\bar{\boldsymbol{q}})\boldsymbol{q}' = \frac{\partial \boldsymbol{q}'}{\partial t} + B_y(\bar{\boldsymbol{q}})D\boldsymbol{q}' + B_z(\bar{\boldsymbol{q}})\frac{\partial \boldsymbol{q}'}{\partial z} + B_2(\bar{\boldsymbol{q}})\Big(D^2\boldsymbol{q}' + \frac{\partial^2 \boldsymbol{q}'}{\partial z^2}\Big) + C(\bar{\boldsymbol{q}})\boldsymbol{q}', \tag{7}$$

The linear terms are now written

$$A(\bar{\boldsymbol{q}})\frac{\partial \boldsymbol{q}'}{\partial x} + B_2(\bar{\boldsymbol{q}})\frac{\partial^2 \boldsymbol{q}'}{\partial x^2} + L(\bar{\boldsymbol{q}})\boldsymbol{q}' = \frac{\partial \boldsymbol{q}'}{\partial t} + \mathcal{N}(\bar{\boldsymbol{q}}, \boldsymbol{q}') + \mathcal{N}(\boldsymbol{q}', \bar{\boldsymbol{q}}),$$

while for the nonlinear terms we define

$$\boldsymbol{F}(\boldsymbol{q}') = -B_y(\boldsymbol{q}')D\boldsymbol{q}' - B_z(\boldsymbol{q}')\frac{\partial \boldsymbol{q}'}{\partial z} - B_2(\boldsymbol{q}')\Big(D^2\boldsymbol{q}' + \frac{\partial^2 \boldsymbol{q}'}{\partial z^2}\Big), \tag{8}$$

so that

$$\boldsymbol{F}(\boldsymbol{q}') - A(\boldsymbol{q}')\frac{\partial \boldsymbol{q}'}{\partial x} - B_2(\boldsymbol{q}')\frac{\partial^2 \boldsymbol{q}'}{\partial x^2} = -\mathcal{N}(\boldsymbol{q}', \boldsymbol{q}').$$

Neglecting the second streamwise derivatives of the disturbance variable (temporarily, as discussed above), we obtain

$$A(\bar{\boldsymbol{q}})\frac{\partial \boldsymbol{q}'}{\partial x} + L(\bar{\boldsymbol{q}})\boldsymbol{q}' = \boldsymbol{F}(\boldsymbol{q}') - A(\boldsymbol{q}')\frac{\partial \boldsymbol{q}'}{\partial x}, \tag{9}$$

which is the nonlinear elliptic stability equation in primitive variables.

B. Transformation to characteristic variables

The nonlinear OWNS solution procedure mimics closely the linear OWNS procedure outlined in [15], which solves the equations in characteristic variables. The operator $A(\bar{\boldsymbol{q}})$ is diagonalized as

$$\tilde{A}(\bar{\boldsymbol{q}}) = T(\bar{\boldsymbol{q}})A(\bar{\boldsymbol{q}})T^{-1}(\bar{\boldsymbol{q}}), \tag{10}$$

and we define the disturbance in characteristic variables

$$\boldsymbol{\phi}(x, y, z, t) = T(\bar{\boldsymbol{q}})\boldsymbol{q}'(x, y, z, t). \tag{11}$$

From now on, we drop the argument to T and assume that it is evaluated at $\bar{\boldsymbol{q}}$. To transform our equation to characteristic variables, we pre-multiply by T and use $\boldsymbol{q}' = T^{-1}\boldsymbol{\phi}$ to obtain

$$TA(\bar{\boldsymbol{q}})\frac{\partial (T^{-1}\boldsymbol{\phi})}{\partial x} + TL(\bar{\boldsymbol{q}})T^{-1}\boldsymbol{\phi} = T\boldsymbol{F}(T^{-1}\boldsymbol{\phi}) - TA(T^{-1}\boldsymbol{\phi})\frac{\partial (T^{-1}\boldsymbol{\phi})}{\partial x}. \tag{12}$$

Using the streamwise derivative

$$\frac{\partial (T^{-1}\boldsymbol{\phi})}{\partial x} = \frac{\partial T^{-1}}{\partial x}\boldsymbol{\phi} + T^{-1}\frac{\partial \boldsymbol{\phi}}{\partial x},$$

we define the linear operator and nonlinear term in characteristic variables

$$\tilde{L}(\bar{q}) = TL(\bar{\boldsymbol{q}})T^{-1} + TA(\bar{\boldsymbol{q}})\frac{\partial T^{-1}}{\partial x},$$
$$\tilde{\boldsymbol{F}}(\boldsymbol{\phi}) = T\boldsymbol{F}(T^{-1}\boldsymbol{\phi}) - TA(T^{-1}\boldsymbol{\phi})\frac{\partial T^{-1}}{\partial x}\boldsymbol{\phi},$$

which results in

$$\tilde{A}(\bar{\boldsymbol{q}} + T^{-1}\boldsymbol{\phi})\frac{\partial \boldsymbol{\phi}}{\partial x} + \tilde{L}(\bar{\boldsymbol{q}})\boldsymbol{\phi} = \tilde{\boldsymbol{F}}(\boldsymbol{\phi}), \tag{13}$$

the nonlinear elliptic stability equation in characteristic variables.

C. Parabolization using the OWNS projection procedure

We wish to apply a spatial-marching procedure to (13), but it is elliptic and supports both upstream- and downstream-going modes, so we will parabolize it using the OWNS projection (OWNS-P) procedure. OWNS-P has been successfully applied to linear-inhomogeneous equations of the form

$$\tilde{A}(\bar{\boldsymbol{q}})\frac{\partial \boldsymbol{\phi}}{\partial x} + \tilde{L}(\bar{\boldsymbol{q}})\boldsymbol{\phi} = \boldsymbol{f}, \tag{14}$$

where $\boldsymbol{f}$ is an arbitrary forcing function. We show below that this approach readily extends to nonlinear equations of the form (13), where the nonlinear terms are treated as a forcing function.

In linear OWNS-P, we isolate $\partial\boldsymbol{\phi}/\partial x$ as

$$\frac{\partial \boldsymbol{\phi}}{\partial x} = M + \boldsymbol{g},$$

for

$$M = -\tilde{A}^{-1}\tilde{L}, \quad \boldsymbol{g} = \tilde{A}^{-1}\boldsymbol{f}.$$

where M has the eigen-decomposition $M = VDV^{-1}$ and the argument $\bar{\boldsymbol{q}}$ has been dropped for brevity. The solution can be expanded as a linear combination of V

$$\boldsymbol{\phi} = V\boldsymbol{\psi} = \sum_{k=1}^{N} \boldsymbol{v}^{(k)}\psi_k,$$

and we can further partition V into its downstream- (V') and upstream-going (V'') components so that

$$\boldsymbol{\phi} = V\boldsymbol{\psi} = \begin{bmatrix} V' & V'' \end{bmatrix} \begin{bmatrix} \boldsymbol{\psi}' \\ \boldsymbol{\psi}'' \end{bmatrix},$$

with the eigenvalues

$$D = \begin{bmatrix} D' & 0 \\ 0 & D'' \end{bmatrix}.$$

Whether an eigenvector is upstream- or downstream-going is determined based on its eigenvalue, according to the well-posedness theory of Kreiss [16], as described in [14]. Here, D' denotes downstream-going eigenvalues, while D'' denotes upstream-going eigenvalues. We use the eigensystem of M to define a projection operator

$$P = V \begin{bmatrix} I & 0 \\ 0 & 0 \end{bmatrix} V^{-1},$$

which retains the downstream-going modes associated with ψ' while removing the upstream-going modes associated with ψ'' such that

$$\boldsymbol{\phi}' = P\boldsymbol{\phi}, \quad \boldsymbol{\phi}'' = [I - P]\boldsymbol{\phi}.$$

Explicitly finding the eigensystem of M is computationally expensive, and we avoid doing so by seeking an approximation to P using a recursive filtering approach to remove the upstream-going modes [14, 15]. We will use the exact projection operator to explain the remainder of the nonlinear OWNS procedure, and then we will discuss how to approximate the projection operator in section II.J.

We use linearity to assert that

$$\frac{\partial \boldsymbol{\phi}'}{\partial x} + \frac{\partial \boldsymbol{\phi}''}{\partial x} = P(\bar{\boldsymbol{q}})[M(\bar{\boldsymbol{q}})\boldsymbol{\phi} + \boldsymbol{g}] + [I - P(\bar{\boldsymbol{q}})][M(\bar{\boldsymbol{q}})\boldsymbol{\phi} + \boldsymbol{g}],$$

and it is shown in [15] that P and M commute so that

$$P(\bar{\boldsymbol{q}})M(\bar{\boldsymbol{q}})\boldsymbol{\phi} = M(\bar{\boldsymbol{q}})P(\bar{\boldsymbol{q}})\boldsymbol{\phi} = M(\bar{\boldsymbol{q}})\boldsymbol{\phi}',$$
$$[I - P(\bar{\boldsymbol{q}})]M(\bar{\boldsymbol{q}})\boldsymbol{\phi} = M(\bar{\boldsymbol{q}})[I - P(\bar{\boldsymbol{q}})]\boldsymbol{\phi} = M(\bar{\boldsymbol{q}})\boldsymbol{\phi}''.$$

The equations can be split in two

$$\frac{\partial \boldsymbol{\phi}'}{\partial x} = M(\bar{\boldsymbol{q}})\boldsymbol{\phi}' + P(\bar{\boldsymbol{q}})\boldsymbol{g},$$
$$\frac{\partial \boldsymbol{\phi}''}{\partial x} = M(\bar{\boldsymbol{q}})\boldsymbol{\phi}'' + [I - P(\bar{\boldsymbol{q}})]\boldsymbol{g},$$

so that we can solve two one-way equations to recover the full elliptic solution as

$$\boldsymbol{\phi}' + \boldsymbol{\phi}'' = P(\bar{\boldsymbol{q}})\boldsymbol{\phi} + [I - P(\bar{\boldsymbol{q}})]\boldsymbol{\phi} = \boldsymbol{\phi}.$$

We will follow a similar procedure to define two nonlinear one-way equations for (13). However, by solving the nonlinear one-way equations separately, we are losing information about how the full elliptic solution affects the nonlinear term

(i.e., $\boldsymbol{F}(\boldsymbol{\phi})$ is different from $\boldsymbol{F}(\boldsymbol{\phi}')$), so we will not able to use linear superposition to recover the full elliptic solution after solving for $\boldsymbol{\phi}'$ and $\boldsymbol{\phi}''$.

We will now define our nonlinear one-way equations. First we rearrange (13) as

$$\frac{\partial \boldsymbol{\phi}}{\partial x} = \tilde{A}(\bar{\boldsymbol{q}})^{-1}[\tilde{L}(\bar{\boldsymbol{q}})\boldsymbol{\phi} + \tilde{A}(T^{-1}\boldsymbol{\phi})\frac{\partial \boldsymbol{\phi}}{\partial x} - \tilde{\boldsymbol{F}}(\boldsymbol{\phi})], \tag{15}$$

and then applying the projection operator results in the following one-way equations

$$\frac{\partial \boldsymbol{\phi}'}{\partial x} = -P(\bar{\boldsymbol{q}})\big(\tilde{A}(\bar{\boldsymbol{q}})^{-1}[\tilde{L}(\bar{\boldsymbol{q}})\boldsymbol{\phi} + \tilde{A}(T^{-1}\boldsymbol{\phi})\frac{\partial \boldsymbol{\phi}}{\partial x} - \tilde{\boldsymbol{F}}(\boldsymbol{\phi})]\big), \tag{16a}$$

$$\frac{\partial \boldsymbol{\phi}''}{\partial x} = -[I - P(\bar{\boldsymbol{q}})]\big(\tilde{A}(\bar{\boldsymbol{q}})^{-1}[\tilde{L}(\bar{\boldsymbol{q}})\boldsymbol{\phi} + \tilde{A}(T^{-1}\boldsymbol{\phi})\frac{\partial \boldsymbol{\phi}}{\partial x} - \tilde{\boldsymbol{F}}(\boldsymbol{\phi})]\big). \tag{16b}$$

Notice that we recover the full elliptic equation if we sum (16a) and (16b) together. Also notice that these equations can give us a stable one-way march, but the full elliptic solution (and its effect on the nonlinear terms) will be unknown if we apply a one-way march, so we must instead consider the equation

$$\frac{\partial \boldsymbol{\phi}'}{\partial x} = -P(\bar{\boldsymbol{q}})\big(\tilde{A}(\bar{\boldsymbol{q}})^{-1}[\tilde{L}(\bar{\boldsymbol{q}})\boldsymbol{\phi}' + \tilde{A}(T^{-1}\boldsymbol{\phi}')\frac{\partial \boldsymbol{\phi}'}{\partial x} - \tilde{\boldsymbol{F}}(\boldsymbol{\phi}')]\big), \tag{17}$$

where we have modified (16a) such that the nonlinear terms depend on $\boldsymbol{\phi}'$ (known) instead of $\boldsymbol{\phi}$ (unknown). We will be missing information about upstream effects on the nonlinear term, but we plan to solve (17) to study convective instabilities, so it is reasonable to assume that the upstream-going modes have a relatively small effect on the overall solution.

D. Spatial marching

Previous work on linear OWNS has used the backward-differentiation formula (BDF) to march the equations in x [10, 11]. We have found that this also works well for nonlinear OWNS, so we apply an s-step BDF scheme to the elliptic equation (13) to obtain

$$\sum_{l=0}^{s-1} c^{(l)} \boldsymbol{\phi}_+^{(k+1-l)} = -\Delta x\big(\tilde{A}(\bar{\boldsymbol{q}}^{(k+1)} + T^{-1}\boldsymbol{\phi}_+^{(k+1)})^{-1}[\tilde{L}(\bar{\boldsymbol{q}}^{(k+1)})\boldsymbol{\phi}_+^{(k+1)} - \tilde{\boldsymbol{F}}(\boldsymbol{\phi}_+^{(k+1)})]\big), \tag{18}$$

which we rearrange as

$$\begin{aligned}\sum_{l=0}^{s-1} c^{(l)} \boldsymbol{\phi}_+^{(k+1-l)} = &-\tilde{A}(\bar{\boldsymbol{q}}^{(k+1)})^{-1}[\Delta x\tilde{L}(\bar{\boldsymbol{q}}^{(k+1)})\boldsymbol{\phi}_+^{(k+1)} \\ &+ \sum_{l=0}^{s-1} c^{(l)}\tilde{A}(T^{-1}\boldsymbol{\phi}_+^{(k+1)})\boldsymbol{\phi}_+^{(k+1-l)} - \Delta x\tilde{\boldsymbol{F}}(\boldsymbol{\phi}_+^{(k+1)})].\end{aligned} \tag{19}$$

This equation is elliptic, so we use the projection operator to obtain

$$\begin{aligned}\sum_{l=0}^{s-1} c^{(l)} \boldsymbol{\phi}_+^{(k+1-l)} = &-P(\bar{\boldsymbol{q}}^{(k+1)})\tilde{A}(\bar{\boldsymbol{q}}^{(k+1)})^{-1}[\Delta x\tilde{L}(\bar{\boldsymbol{q}}^{(k+1)})\boldsymbol{\phi}_+^{(k+1)} \\ &+ \sum_{l=0}^{s-1} c^{(l)}\tilde{A}(T^{-1}\boldsymbol{\phi}_+^{(k+1)})\boldsymbol{\phi}_+^{(k+1-l)} - \Delta x\tilde{\boldsymbol{F}}(\boldsymbol{\phi}_+^{(k+1)})],\end{aligned} \tag{20}$$

which is a parabolic equation that supports only downstream-going modes.

E. Equations in Fourier space

If the disturbances are periodic in time with frequency ω and in the spanwise direction with wavenumber β, then they can be represented using a truncated Fourier series

$$\boldsymbol{\phi}(x, y, z, t) = \sum_{m=-M}^{M}\sum_{n=-N}^{N} \hat{\boldsymbol{\phi}}_{mn}(x, y)e^{i(n\beta z - m\omega t)}. \tag{21}$$

The disturbance must be real-valued, so that we must have $(\hat{\boldsymbol{\phi}}_{-m,-n})^* = \hat{\boldsymbol{\phi}}_{mn}$, where $(\cdot)^*$ denotes the complex conjugate. Therefore, we need only solve $(M+1)\times(2N+1)$ equations instead of $(2M+1)\times(2N+1)$ equations since roughly half of the equations are redundant. When desired, we can further reduce the number of equations to $(M+1)\times(N+1)$ by employing a symmetry condition in z, as described in section II.G

In linear OWNS (for waves of infinitesimal amplitude), the nonlinear terms are neglected and all Fourier modes (m,n) evolve independently of each other so that we can consider each mode separately as

$$\sum_{l=0}^{s-1} c^{(l)} \hat{\boldsymbol{\phi}}_{mn}^{(k+1-l)} = -\Delta x P_{mn}(\bar{\boldsymbol{q}}^{(k+1)}) \tilde{A}^{-1}(\bar{\boldsymbol{q}}^{(k+1)}) \tilde{L}_{mn}(\bar{\boldsymbol{q}}^{(k+1)}) \hat{\boldsymbol{\phi}}_{mn}^{(k+1)},$$

for the linear operator

$$\tilde{L}_{mn} = -im\omega I + TB_y DT^{-1} + in\beta TB_z T^{-1} + TB_2 T^{-1}[D^2 - n^2\beta^2 I] + TCT^{-1} + TA\frac{\partial T^{-1}}{\partial x}, \tag{22}$$

for $m = -M,\ldots,M$ and $n = -N,\ldots,N$. However, in nonlinear OWNS (for waves of finite amplitude) the nonlinear terms are no longer negligible and all Fourier modes (m,n) become coupled. We will compute the Fourier components of the nonlinear terms so that we can solve (20) in Fourier space.

We define a nonlinear marching term

$$\tilde{\boldsymbol{G}}(\boldsymbol{\phi}_+^{(k+1)},\ldots,\boldsymbol{\phi}_+^{(k+2-s)}) = \sum_{l=0}^{s-1} \tilde{A}(T^{-1}\boldsymbol{\phi}_+^{(k+1)})\boldsymbol{\phi}_+^{(k+1-l)}, \tag{23}$$

and expand the nonlinear terms in a Fourier series

$$\tilde{\boldsymbol{F}}(\boldsymbol{\phi}_+^{(k+1)}) = \sum_{m=-M}^{M}\sum_{n=-N}^{N} \hat{\boldsymbol{F}}_{mn}^{(k+1)} e^{i(n\beta z - m\omega t)}, \tag{24}$$

$$\tilde{\boldsymbol{G}}(\boldsymbol{\phi}_+^{(k+1)},\ldots,\boldsymbol{\phi}_+^{(k+2-s)}) = \sum_{m=-M}^{M}\sum_{n=-N}^{N} \hat{\boldsymbol{G}}_{mn}^{(k+1)} e^{i(n\beta z - m\omega t)}. \tag{25}$$

Finally, we use the orthogonality of $e^{i(n\beta z - m\omega t)}$ to get $(2M+1)\times(2N+1)$ equations (where some equations are redundant, as described above)

$$\sum_{l=0}^{s-1} c^{(l)} \hat{\boldsymbol{\phi}}_{mn}^{(k+1-l)} = -P_{mn}(\bar{\boldsymbol{q}}^{(k+1)})\tilde{A}(\bar{\boldsymbol{q}}^{(k+1)})^{-1}[\Delta x \tilde{L}_{mn}(\bar{\boldsymbol{q}}^{(k+1)})\hat{\boldsymbol{\phi}}_{mn}^{(k+1)} + \hat{\boldsymbol{G}}_{mn}^{(k+1)} - \Delta x \hat{\boldsymbol{F}}_{mn}^{(k+1)}], \tag{26}$$

for all $m = -M,\ldots,M$ and $n = -N,\ldots,N$. We see that nonlinear OWNS results in a system of linear OWNS equations that are coupled through the nonlinear terms.

The Fourier series of the nonlinear terms is computed using a pseudo-spectral approach. The variables are first transformed to physical space using the inverse Fast Fourier Transform, and the nonlinear products are formed in the physical space. The nonlinear term is then transformed back to Fourier space and dealiased using the 3/2 rule.

F. Special treatment of the zero-frequency modes

Linear OWNS has been applied extensively to cases where $\omega \neq 0$ (i.e., non-zero temporal frequency), but it has been used less extensively for cases where $\omega = 0$ (i.e., zero temporal frequency). Previous work has used linear OWNS to study cases with $\omega = 0$ by choosing a small temporal frequency such that $|\omega| > 0$. In particular, this approach has been used to study streaks in boundary layer flows [12].

This approach works well for linear OWNS, but we have not yet been able to robustly adapt it to the nonlinear case. For now, we consider an alternative approach developed for PSE to avoid projecting the zero-frequency modes. Namely, the zero frequency equation is parabolized by neglecting the streamwise pressure gradient ($\partial\hat{p}_{0,n}/\partial x$) and the streamwise diffusion terms ($\partial^2\hat{\boldsymbol{q}}_{0,n}/\partial x^2$). Future work will investigate how to project properly the zero-frequency modes for nonlinear OWNS such that this *ad hoc* treatment is eliminated.

G. Spanwise symmetry

For the test cases we study here, the disturbance variable is constrained to be symmetric in the spanwise (z) direction, and the number of equations can be reduced. In primitive variables, all variables have even-symmetry, with the exception of the w-velocity which has odd-symmetry,

$$\begin{aligned}\hat{\nu}_{m,-n} &= \hat{\nu}_{m,n},\\ \hat{u}_{m,-n} &= \hat{u}_{m,n},\\ \hat{v}_{m,-n} &= \hat{v}_{m,n},\\ \hat{w}_{m,-n} &= -\hat{w}_{m,n},\\ \hat{p}_{m,-n} &= \hat{p}_{m,n}.\end{aligned}$$

H. Boundary conditions

At the wall, we impose no-slip isothermal boundary conditions ($u' = v' = w' = T' = 0$), while we solve for the specific volume, ν', at the wall using the (nonlinear) continuity equation. At the far-field boundary, we impose 1D (in y) inviscid Thompson characteristic boundary conditions to prevent spurious numerical reflections [17]. The inviscid assumption is valid because viscous effects from the boundary layer are negligible in the far-field. This choice of boundary conditions matches the boundary conditions used previously for linear OWNS [10, 11]. The Thompson characteristic boundary condition (as implemented in our code) is based on the linearized Navier-Stokes equations. However, this choice is reasonable because nonlinear effects are negligible far from the boundary layer.

Some previous work on PSE has used characteristic boundary conditions in the far-field [8]. However, other previous work on PSE has used the far-field boundary condition $\hat{\boldsymbol{q}}'_{mn}(y_{\max}) = 0$ [18]. The boundary layer must be allowed to grow in the wall-normal direction (due to nonlinear interactions), so we cannot have $\hat{v}'_{00}(y_{\max}) = 0$ for the mean-flow distortion (MFD). Instead, we must use either characteristic boundary conditions, or choose $\partial\hat{v}'_{00}/\partial y = 0$ at $y_{\max}$. The characteristic far-field boundary conditions are advantageous because they allow us to use the same boundary conditions for all modes, instead of handling the MFD as a separate case.

I. Streamwise diffusion terms

As noted above, neglecting the streamwise diffusion terms simplifies the parabolization procedure. Moreover, previous work on linear OWNS has reintroduced these terms (approximately) after parabolizing the equations, and found that their inclusion did not affect significantly the results of the stability calculation [11]. However, we have found that their impact on nonlinear OWNS is more pronounced, so we include them by discretizing second-streamwise derivatives using a second-order backward difference scheme, which is similar to the procedure used previously for linear OWNS [11]. Provided the resulting equations are stable (which we verify *a posteriori*), then, apart from the parabolization error, the streamwise terms are included to $O(\Delta x^2)$.

Thus we discretize the second-derivative of $\hat{\boldsymbol{\phi}}_{mn}$ using a second-order backward difference as

$$\left.\frac{\partial^2\hat{\boldsymbol{\phi}}_{mn}}{\partial x^2}\right|_{x=x^{(k+1)}} \approx \frac{\hat{\boldsymbol{\phi}}_{mn}^{(k+1)} - 2\hat{\boldsymbol{\phi}}_{mn}^{(k)} + \hat{\boldsymbol{\phi}}_{mn}^{(k-1)}}{(\Delta x)^2}. \tag{27}$$

Defining

$$\hat{\boldsymbol{H}}_{mn}^{(k+1)} = TB_2(\bar{\boldsymbol{q}})\left(T^{-1}\frac{\boldsymbol{\phi}_{mn}^{(k+1)} - 2\boldsymbol{\phi}_{mn}^{(k)} + \boldsymbol{\phi}_{mn}^{(k-1)}}{\Delta x} + 2\sum_{l=0}^{s-1} c^{(l)}\frac{\partial T^{-1}}{\partial x}\hat{\boldsymbol{\phi}}_{mn}^{(k+1-l)} + \Delta x\frac{\partial^2 T^{-1}}{\partial x^2}\boldsymbol{\phi}_{mn}^{(k+1)}\right)$$

we can write

$$\sum_{l=0}^{s-1} c^{(l)}\hat{\boldsymbol{\phi}}_{mn}^{(k+1-l)} = -P_{mn}(\bar{\boldsymbol{q}}^{(k+1)})\tilde{A}^{-1}(\bar{\boldsymbol{q}}^{(k+1)})[\Delta x\tilde{L}_{mn}(\bar{\boldsymbol{q}}^{(k+1)})\hat{\boldsymbol{\phi}}_{mn}^{(k+1)} + \hat{\boldsymbol{H}}_{mn}^{(k+1)} + \hat{\boldsymbol{G}}_{mn}^{(k+1)} - \Delta x\hat{\boldsymbol{F}}_{mn}^{(k+1)}]. \tag{28}$$

which constitutes the final set of (exact) equations we solve in nonlinear OWNS.

J. Approximate projection operator

Constructing the exact projection operator, $P_{mn}(\bar{\boldsymbol{q}})$, requires the eigen-decomposition of $M_{mn}(\bar{\boldsymbol{q}}) = \tilde{A}^{-1}(\bar{\boldsymbol{q}})\tilde{L}_{mn}(\bar{\boldsymbol{q}})$ which is computationally expensive and can be avoided by employing the recursive filtering approach described in [15]. Given the (real-valued) diagonal operator $\tilde{A}(\bar{\boldsymbol{q}})$, we identify the N_+ positive entries $\tilde{A}_{++}(\bar{\boldsymbol{q}})$, the N_- negative entries $\tilde{A}_{--}(\bar{\boldsymbol{q}})$, and the N_0 zero entries $\tilde{A}_{00}(\bar{\boldsymbol{q}}) = 0$, such that $N_+ + N_- + N_0 = N_y \cdot N_{\text{dim}}$, where N_y is the number of grid-point in y and N_{dim} is the number of flow quantities (4 in 2D and 5 in 3D). We further define the components $\hat{\boldsymbol{\phi}}_{+,mn}$, $\hat{\boldsymbol{\phi}}_{-,mn}$, and $\hat{\boldsymbol{\phi}}_{0,mn}$ of $\hat{\boldsymbol{\phi}}_{mn}$. If $N_0 > 0$, then $\tilde{A}(\bar{\boldsymbol{q}})$ is singular: for a subsonic boundary layer flow, $\tilde{A}(\bar{q})$ is singular only at the wall (after discretization) due to the boundary conditions ($\bar{u} = 0$ at the wall).

It is shown in [15] that applying the following equations

$$\hat{\boldsymbol{\phi}}_{+,mn}^{-(N_b)} = 0 \tag{29a}$$

$$(\tilde{L}_{mn} - i\beta_-^{(j)}\tilde{A})\hat{\boldsymbol{\phi}}_{mn}^{(-j)} - (\tilde{L}_{mn} - i\beta_+^{(j)}\tilde{A})\hat{\boldsymbol{\phi}}_{mn}^{(-j-1)} = 0, \quad j = 1, \ldots, N_b - 1 \tag{29b}$$

$$(\tilde{L}_{mn} - i\beta_-^{(0)}\tilde{A})\hat{\boldsymbol{\phi}}_{mn}^{(0)} - (\tilde{L}_{mn} - i\beta_+^{(0)}\tilde{A})\hat{\boldsymbol{\phi}}_{mn}^{(-1)} = (\tilde{L}_{mn} - i\beta_-^{(0)}\tilde{A})\hat{\boldsymbol{\phi}}_{mn} \tag{29c}$$

$$\tilde{L}_{0\pm,mn}\hat{\boldsymbol{\phi}}_{\pm,mn}^{(0)} + \tilde{L}_{00,mn}\hat{\boldsymbol{\phi}}_{0,mn}^{(0)} = 0 \tag{29d}$$

$$(\tilde{L}_{mn} - i\beta_+^{(j)}\tilde{A})\hat{\boldsymbol{\phi}}_{mn}^{(j)} - (\tilde{L}_{mn} - i\beta_-^{(j)}\tilde{A})\hat{\boldsymbol{\phi}}_{mn}^{(j+1)} = 0, \quad j = 0, \ldots, N_b - 1 \tag{29e}$$

$$\hat{\boldsymbol{\phi}}_{-,mn}^{(N_b)} = 0, \tag{29f}$$

to the elliptic variable $\hat{\boldsymbol{\phi}}_{mn}$ results in the parabolic variable $\hat{\boldsymbol{\phi}}_{mn}^{(0)}$. Here, $\{\beta_\pm^{(j)}\}_{j=0}^{N_b-1}$ are termed the *recursion parameters*, while $\{\hat{\boldsymbol{\phi}}_{mn}^{(j)}\}_{j=-N_b}^{N_b}$ are termed the *auxiliary variables*; the recursion parameter selection for subsonic boundary layer flows is described in appendix IV.B. The action of the approximate projection operator on $\hat{\boldsymbol{\phi}}_{mn}$ can be represented compactly as

$$\hat{\boldsymbol{\phi}}_{mn}^{(0)} = P_3\boldsymbol{\phi}_{\text{aux}},$$
$$P_{2,mn}\boldsymbol{\phi}_{\text{aux}} = P_{1,mn}\hat{\boldsymbol{\phi}}_{mn},$$

where P_1 represents the right-hand-side of (29), P_2 represents the left-hand-side, and P_3 extracts $\hat{\boldsymbol{\phi}}_{mn}^{(0)}$ from $\boldsymbol{\phi}_{\text{aux}}$. The projection operator can also be applied approximately using the OWNS recursive (OWNS-R) approach [19], which entails a lower computational cost than OWNS-P. We chose to develop nonlinear OWNS using the OWNS-P approach because we found it be more robust, but the computational cost of nonlinear OWNS could be decreased by employing the OWNS-R approach.

To solve (approximately) the nonlinear OWNS equation (28), we re-order our operators such that

$$\tilde{A} = \begin{bmatrix} \tilde{A}_{\pm\pm} & 0 \\ 0 & 0 \end{bmatrix}, \quad \tilde{L}_{mn} = \begin{bmatrix} \tilde{L}_{\pm\pm,mn} & \tilde{L}_{\pm 0,mn} \\ \tilde{L}_{0\pm,mn} & \tilde{L}_{00,mn} \end{bmatrix}, \quad \hat{\boldsymbol{b}}_{mn} = \begin{bmatrix} \hat{\boldsymbol{b}}_{\pm,mn} \\ \hat{\boldsymbol{b}}_{0,mn} \end{bmatrix},$$

for the nonlinear term

$$\hat{\boldsymbol{b}}_{mn} = \hat{\boldsymbol{H}}_{mn} + \hat{\boldsymbol{G}}_{mn} - \Delta x\hat{\boldsymbol{F}}_{mn},$$

where $N_\pm = N_+ + N_-$ as in [15]. These operators define

$$E = \begin{bmatrix} I_{\pm\pm} & 0 \\ 0 & 0 \end{bmatrix}, \quad M_{mn} = \begin{bmatrix} \tilde{A}_{\pm\pm}^{-1}\tilde{L}_{\pm\pm,mn} & \tilde{A}_{\pm\pm}^{-1}\tilde{L}_{\pm 0,mn} \\ \tilde{L}_{0\pm,mn} & \tilde{L}_{00,mn} \end{bmatrix}, \quad \hat{\boldsymbol{d}}_{mn} = \begin{bmatrix} \tilde{A}_{\pm\pm}^{-1}\hat{\boldsymbol{b}}_{\pm,mn} \\ \hat{\boldsymbol{b}}_{0,mn} \end{bmatrix},$$

and for singular $\tilde{A}$, equation (28) becomes

$$\sum_{l=0}^{s-1} c^{(l)} E\hat{\boldsymbol{\phi}}_{mn}^{(k+1-l)} = -P_{mn}(\bar{\boldsymbol{q}}^{(k+1)})[\Delta x M_{mn}(\bar{\boldsymbol{q}})\hat{\boldsymbol{\phi}}_{mn}^{(k+1)} + \hat{\boldsymbol{d}}_{mn}^{(k+1)}],$$

where $P_{mn}(\bar{\boldsymbol{q}}^{(k+1)})$ is still the exact projection operator. The approximate projection operator is applied by writing

$$\sum_{l=0}^{s-1} c^{(l)} E\hat{\boldsymbol{\phi}}_{mn}^{(k+1-l)} = P_3\boldsymbol{\phi}_{\text{aux}}$$
$$P_{2,mn}\boldsymbol{\phi}_{\text{aux}} = -P_{1,mn}[\Delta x M_{mn}(\bar{\boldsymbol{q}})\hat{\boldsymbol{\phi}}_{mn}^{(k+1)} + \hat{\boldsymbol{d}}_{mn}^{(k+1)}],$$

for each mode (m, n).

Next we define the expanded state vector

$$\boldsymbol{\phi}^{\ddagger}_{mn} = \begin{bmatrix} \hat{\boldsymbol{\phi}}_{mn} \\ \boldsymbol{\phi}_{\text{aux}} \end{bmatrix},$$

and the associated operators

$$A^{\ddagger} = \begin{bmatrix} E & 0 \\ 0 & 0 \end{bmatrix}, \quad M^{\ddagger}_{mn} = \begin{bmatrix} 0 & -P_3 \\ \Delta x P_{1,mn} M_{mn} & P_{2,mn} \end{bmatrix}, \quad \hat{\boldsymbol{d}}^{\ddagger}_{mn} = \begin{bmatrix} 0 \\ -P_{1,mn}\hat{\boldsymbol{d}}_{mn} \end{bmatrix}.$$

These operators allow us to write

$$[c^{(0)}A^{\ddagger} + M^{\ddagger}_{mn}]\boldsymbol{\phi}^{(k+1)\ddagger}_{mn} = \hat{\boldsymbol{d}}^{\ddagger}_{mn} - \sum_{l=1}^{s-1} c^{(l)} E \hat{\boldsymbol{\phi}}^{(k+1-l)\ddagger}_{mn}, \quad m = -M, \ldots, M, \quad n = -N, \ldots, N, \tag{30}$$

which represents the approximate implementation of 28.

K. Solution procedure

Equation (30) comprises a block-diagonal system of equations where the modes (m, n) are coupled only through the nonlinear terms on the right-hand-side. We converge this system of equations using a quasi-Newton method where the Jacobian depends only on the linear terms. This reduces the computational cost because instead of inverting one large matrix that couples all of the modes together, we invert $(M + 1) \times (N + 1)$ smaller matrices (one for each mode). Moreover, the Jacobian does not depend on the solution variable, so we perform the LU-decomposition of the Jacobian matrix for each mode (m, n) once (at each step of the march), and then solve this system iteratively until the residual converges to the desired tolerance. The dominant computational cost is the LU-decompositions, which are independent for all modes, so that the computational cost scales linearly in the number of modes.

III. Validation

We validate our nonlinear OWNS solver by applying it to 2D and 3D Blasius boundary layer flows for which there are existing DNS and PSE results in the literature.

A. 2D Blasius boundary layer

To validate our 2D nonlinear OWNS (NOWNS) solver, we consider the incompressible test case developed in [7]. In this test case, we use the Tollmien-Schlichting (TS) wave from parallel linear stability theory (LST) as the inlet boundary condition, and we march downstream to study its nonlinear evolution. This case has been widely studied in the literature using both nonlinear PSE (NPSE) and DNS, and we will compare our results to those presented in [20].

To approach the incompressible limit, we choose the Mach number $Ma = 0.1$, while we use the dimensionless temporal frequency $F = \omega^* \nu^*_\infty / U^{*2}_\infty = 86 \times 10^{-6}$, where $(\cdot)^*$ denotes a dimensional quantity. In 2D, we define the amplitude, based on the maximum u-velocity, as

$$u'^{(0)}_{\max}(x) = \max_y |u'_0(x, y)|, \quad u'^{(i)}_{\max}(x) = \max_y \sqrt{2}|u'_i(x, y)|, \quad i = 1, \ldots, M.$$

Then we specify the inlet amplitude $u'^{(1)}_{\max}(x_0) = 0.25\%$ for the TS wave at $R = 400$, for the streamwise coordinate $R = \sqrt{U^*_\infty x^*/\nu^*_\infty}$. All other Fourier components initially have zero-amplitude and are generated through nonlinear interactions with the TS wave. The grid extends over the domain $R \in [400, 1000]$ and $y \in [0, 75]$ with 4000 stations evenly spaced in x and 150 grid points in y, with the majority of the grid points clustered towards the wall, while the Fourier series is truncated at $M = 5$ temporal modes (increasing M further does not modify significantly the results). The equations are marched using the two-step BDF scheme (BDF2).

In figure 1 we plot the maximum amplitude of the u-velocity perturbation as a function of the streamwise coordinate. We plot the DNS data from [20], and the nonlinear OWNS data from the present study. In figures 2 and 3 we plot the u- and v-velocity profiles for the MFD and the TS wave. We compare the nonlinear OWNS profiles from the present study to the NPSE and DNS profiles computed in [20]. We see that the OWNS profiles agree with the NPSE profiles, which

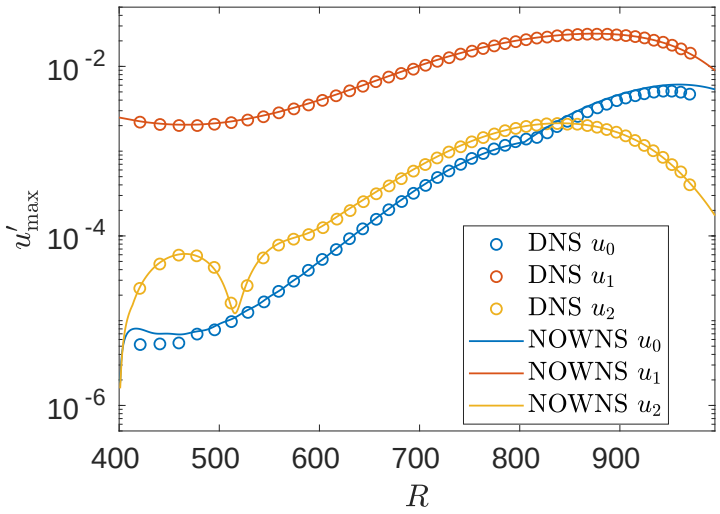

Fig. 1 Amplitude of u' v.s. streamwise coordinate, R, for a TS waves at frequency $F = 86 \times 10^{-6}$ with initial amplitude of $u'^{(1)}_{\max}(x_0) = 0.25\%$.

differ slightly from the DNS profiles because the far-field boundary conditions are implemented differently for DNS. Our nonlinear OWNS solver uses a characteristic boundary condition for v'_0, while the NPSE solver used in [20] uses a Neumann boundary condition, and the two approaches yield similar results despite the different implementations of the boundary conditions.

B. 3D oblique-wave breakdown

We consider the oblique-wave breakdown case studied by [20], where the march is initialized with four oblique waves $(1,1)$, $(1,-1)$, $(-1,1)$ and $(-1,-1)$, which are obtained from LST. The march starts at $R = 523$ with amplitude $u'^{(1,1)}_{\max}(x_0) = \sqrt{2} \times 10^{-3}$ for all four waves, where we have defined the amplitudes

$$
\begin{aligned}
u'^{(0,0)}_{\max}(x) &= \max_y |u'_{0,0}(x,y)|, \\
u'^{(m,0)}_{\max}(x) &= \max_y \sqrt{2}|u'_{m,0}(x,y)|, \quad m = 1,\ldots,M, \\
u'^{(0,n)}_{\max}(x) &= \max_y \sqrt{2}|u'_{0,n}(x,y)|, \quad n = 1,\ldots,N, \\
u'^{(m,n)}_{\max}(x) &= \max_y 2\sqrt{2}|u'_{m,n}(x,y)|, \quad m = 1,\ldots,M, \quad n = 1,\ldots,N,
\end{aligned}
$$

to be consistent with the scaling used in [20]. Here, (m,n) denotes the mode with temporal frequency $m\omega$ and spanwise wavenumber $n\beta$. The oblique waves interact to excite higher modes and to distort the mean flow. The grid extends over the domain $R \in [523, 780]$ and $y \in [0, 75]$ with 2000 stations evenly spaced in x and 150 grid points in y, with the majority of the grid points clustered towards the wall, while the Fourier series is truncated at $M = 3$ temporal modes and $N = 4$ spanwise modes. For the chosen amplitude, increasing the number of Fourier modes does not change the results significantly. As in the 2D test case, we march the equations using the BDF2 scheme.

We consider the frequency $F = 86 \times 10^{-6}$ and the spanwise wavenumber $b = \beta^* \nu^*_\infty / U^*_\infty \times 10^3 = 2/9$ and we plot the amplitudes of the u-velocity as a function of streamwise station in figure 4. We see that we have excellent agreement between the amplitudes predicted by the nonlinear OWNS calculation, and those reported for the DNS calculation. We also plot in figure 5 the u-velocity profiles predicted by NOWNS and DNS at $R = 685$ for the MFD (figure 5a), the oblique mode (figure 5b), the vortex mode (figure 5c), and the first harmonic of the oblique mode in z (figure 5d). We see that we have excellent agreement for between the DNS and NOWNS results for all for modes, which provides further evidence that the nonlinear OWNS approach is implemented correctly.

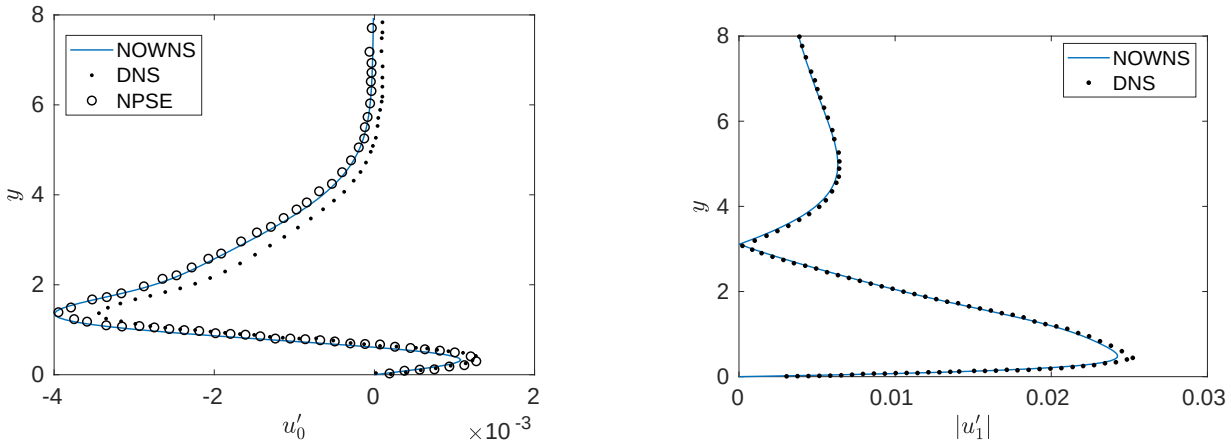

(a) MFD **(b) TS wave**

Fig. 2 u-velocity profiles at streamwise coordinate $R = 883$ for 2D evolution of TS wave.

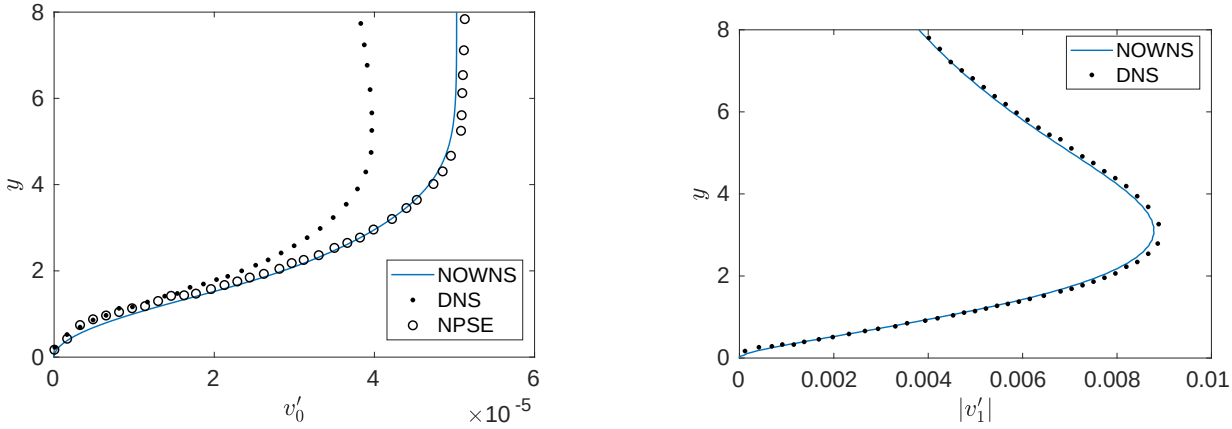

(a) MFD **(b) TS wave**

Fig. 3 v-velocity profiles at streamwise coordinate $R = 883$ for 2D evolution of TS wave.

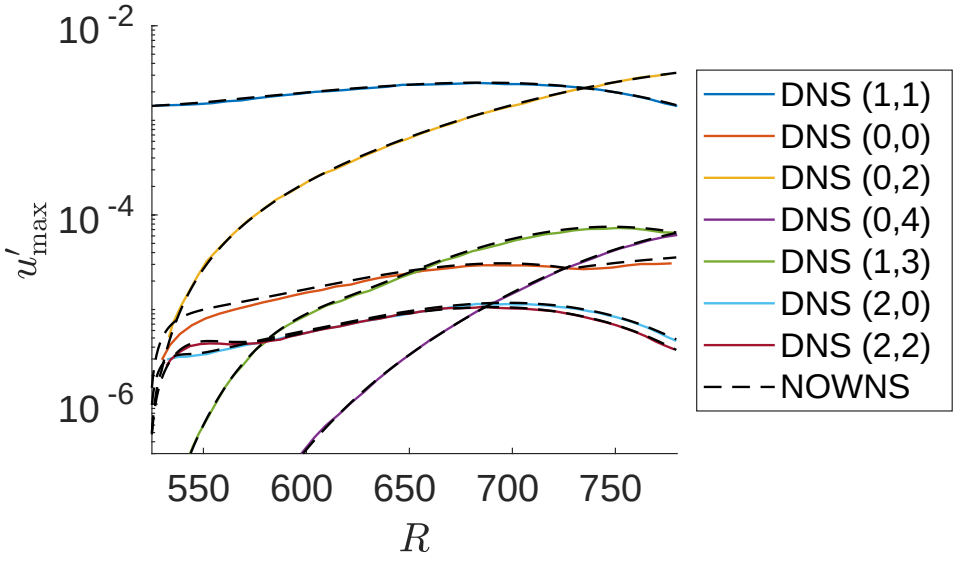

Fig. 4 Amplitude of u' v.s. streamwise coordinate, R, for oblique-wave breakdown at frequency $F = 86 \times 10^{-6}$, spanwise wavenumber $b = 2/9$, with initial amplitude of $u'^{(1,1)}_{\max}(x_0) = \sqrt{2} \times 10^{-3}$.

IV. Conclusion

We have extended the OWNS approach, a fast marching procedure previously developed for solving linear flow disturbance equations, to support nonlinear interactions. We have demonstrated that it is effective for 2D and 3D disturbances in a wall-bounded flow by comparing against previous DNS and nonlinear PSE results.

While the present study only reproduces results for which nonlinear PSE is already effective (with a lower computational cost than nonlinear OWNS), we expect that the nonlinear OWNS approach will permit us to push these calculations further downstream into the transitional regime. The reasons for this optimism are twofold: firstly, OWNS accurately tracks all downstream-propagating disturbances in the flow, not just those at the dominant wavelength, and, secondly, the OWNS approach permits arbitrarily small step sizes. In nonlinear PSE, it is observed that it is not possible to converge the equations past a certain level of nonlinearity because the smaller step size required to converge the nonlinear terms violates the minimum step size required for the parabolization to be stable. In the absence of this restriction, the expectation is that OWNS will still provide accurate solutions provided a sufficiently large number of frequencies and spanwise wavenumbers are retained in the calculations. Demonstrating this superiority is the focus of our future work.

Appendices

A. Linearized Navier-Stokes Operators

Here we present the operators for the Navier-Stokes equations. The operators for the first derivatives, A, B_y, and B_z, are given by

$$A(\boldsymbol{q}) = \begin{bmatrix} u & -\nu & 0 & 0 & 0 \\ 0 & u & 0 & 0 & 0 \\ 0 & 0 & u & 0 & 0 \\ 0 & 0 & 0 & u & 0 \\ 0 & \gamma p & 0 & 0 & u \end{bmatrix}, \quad B_y(\boldsymbol{q}) = \begin{bmatrix} v & 0 & -\nu & 0 & 0 \\ 0 & v & 0 & 0 & 0 \\ 0 & 0 & v & 0 & 0 \\ 0 & 0 & 0 & v & 0 \\ 0 & 0 & \gamma p & 0 & v \end{bmatrix}, \quad B_z(\boldsymbol{q}) = \begin{bmatrix} w & 0 & 0 & -\nu & 0 \\ 0 & w & 0 & 0 & 0 \\ 0 & 0 & w & 0 & 0 \\ 0 & 0 & 0 & w & 0 \\ 0 & 0 & 0 & \gamma p & w \end{bmatrix},$$

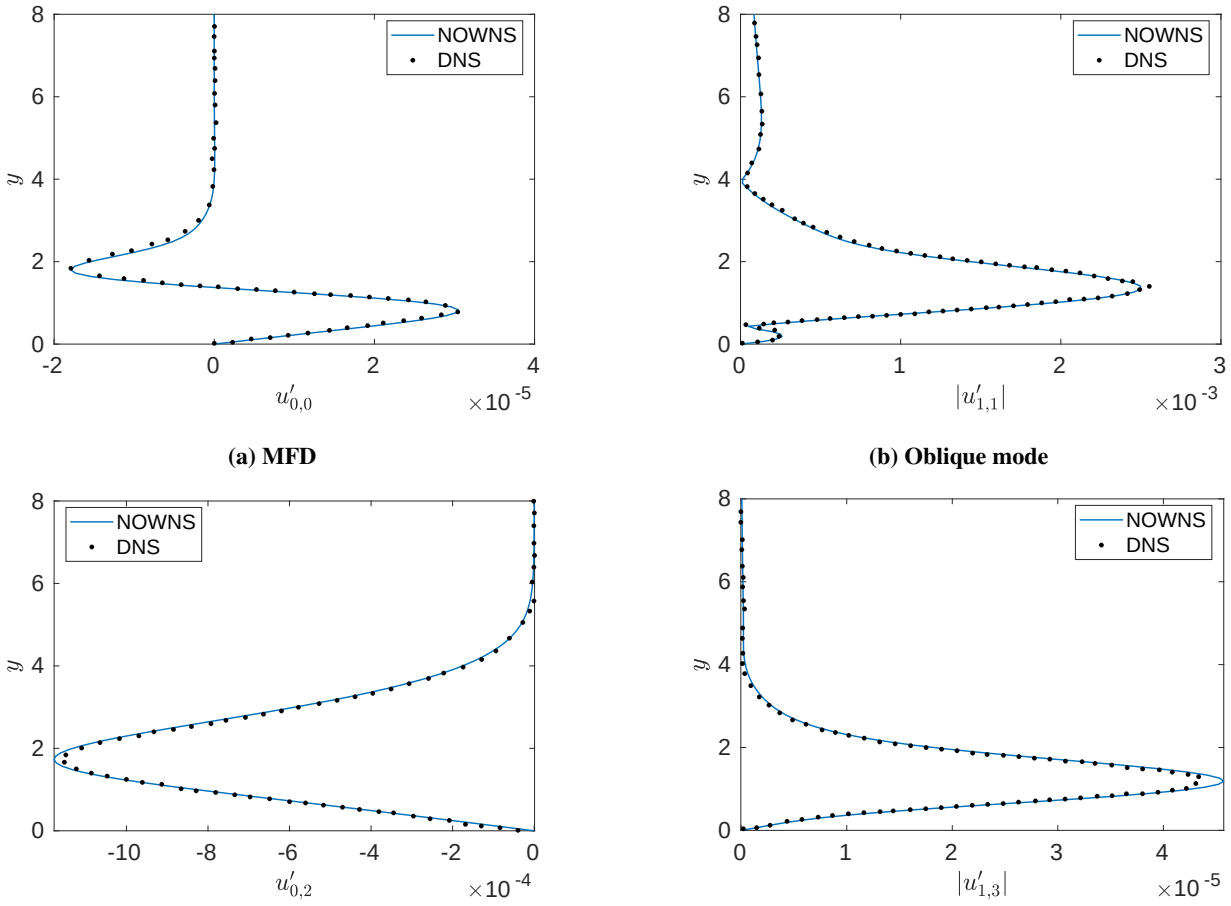

(a) MFD **(b) Oblique mode**

(c) Vortex mode **(d) First harmonic of oblique mode in z**

Fig. 5 u-velocity profiles at streamwise coordinate $R = 685$ for oblique-wave breakdown.

while the operator for the second derivative, B_2, is given by

$$B_2(\boldsymbol{q}) = \begin{bmatrix} 0 & 0 & 0 & 0 & 0 \\ 0 & -\frac{\nu}{Re} & 0 & 0 & 0 \\ 0 & 0 & -\frac{\nu}{Re} & 0 & 0 \\ 0 & 0 & 0 & -\frac{\nu}{Re} & 0 \\ -\frac{\gamma p}{RePr} & 0 & 0 & 0 & -\frac{\gamma\nu}{RePr} \end{bmatrix}.$$

Finally, the operator C that we get using the Reynolds decomposition is given by

$$C(\boldsymbol{q}) = \begin{bmatrix} -\nabla\cdot\boldsymbol{u} & \frac{\partial\nu}{\partial x} & \frac{\partial\nu}{\partial y} & \frac{\partial\nu}{\partial z} & 0 \\ \frac{\partial p}{\partial x} - \frac{1}{Re}\nabla^2 u & \frac{\partial u}{\partial x} & \frac{\partial u}{\partial y} & \frac{\partial u}{\partial z} & 0 \\ \frac{\partial p}{\partial y} - \frac{1}{Re}\nabla^2 v & \frac{\partial v}{\partial x} & \frac{\partial v}{\partial y} & \frac{\partial v}{\partial z} & 0 \\ \frac{\partial p}{\partial z} - \frac{1}{Re}\nabla^2 w & \frac{\partial w}{\partial x} & \frac{\partial w}{\partial y} & \frac{\partial w}{\partial z} & 0 \\ -\frac{\gamma}{RePr}\nabla^2 p & \frac{\partial p}{\partial x} & \frac{\partial p}{\partial y} & \frac{\partial p}{\partial z} & \gamma\nabla\cdot\boldsymbol{u} - \frac{\gamma}{RePr}\nabla^2\nu \end{bmatrix}.$$

B. Recursion parameter sets

The recursion parameters are chosen based on the eigenvalues of the Euler equations linearized about a uniform flow, as described in [14]. The eigenvalues are

$$i\alpha_c = \frac{ik}{\bar{M}_x}, \quad i\alpha_{a_1}(z) = ik\frac{-\bar{M}_x + \mu(z)}{1-\bar{M}_x^2}, \quad i\alpha_{a_2}(z) = ik\frac{-\bar{M}_x - \mu(z)}{1-\bar{M}_x^2},$$

where $\bar{M}_x = \bar{u}/\bar{c}$ is the local streamwise Mach number, $k = \omega/\bar{c}$ is the streamwise wave number, z is a composite wave-number (for the transverse directions), and the function $\mu(z)$ is given by

$$\mu(z) = \sqrt{1-(1-\bar{M}_x^2)z^2}.$$

For subsonic boundary layer flows, we use the same recursion parameters as in [10], which differ slightly from those developed originally in [14], so we will briefly explain the new choice of recursion parameters.

The present choice of recursion parameters are separated into the following groups: (i) vortical modes, which replace convective modes, (ii) fast and slow stream evanescent acoustic modes, and (iii) fast and slow stream propagating acoustic modes, where fast stream modes are associated with the free-stream streamwise Mach number, while slow stream modes are associated with a small Mach number (inside the boundary layer). The recursion parameters for the vortical modes of the present study match closely the parameters for convective modes in [14], while the recursion parameters for the propagating acoustic modes are distributed the same way in both the present study and in [14]. The parameters for the evanescent acoustic modes are distributed in a slightly different way, so we focus our discussion on these parameters.

To distribute the parameters for the evanescent acoustic modes, we define

$$\eta_c = \frac{k}{1-\bar{M}_x}, \quad \eta_m = 1.5\frac{L_y}{\Delta y},$$

where L_y is the (dimensionless) extent of the domain in the wall-normal direction, while Δy is the (uniform) wall-normal grid-spacing. These define the spacing parameter

$$\eta^{(h)} = \eta_m + \frac{h}{N_e-1}\left(\eta_c + 0.1\frac{\eta_m-\eta_c}{N_e-1} - \eta_m\right), \quad h = 0,\ldots,N_e-1,$$

which in turn defines

$$\mu^{(h)} = \mu(\eta^{(h)}), \quad h = 0,\ldots,N_e-1.$$

This contrasts with the choice

$$\mu^{(h)} = \mu_{\max}\frac{h}{2N_e}, \quad h = 0,\ldots,2N_e-1,$$

used in [14], where $\mu_{\max} = \mu(z_{\max})$. Here, $z_{\max}$ represents the maximum transverse wave number supported by the semi-discrete Euler equations (wave numbers larger than $z_{\max}$ need not be considered because they are not supported by the semi-discrete equations). The present approach considers a range of z near $z_{\max}$ (distributed according to $\eta^{(h)}$) which is then used to define $\mu^{(h)}$, while the approach presented in [14] considers only one z to get $\mu_{\max}$, which is then used to define $\mu^{(h)}$ spaced linearly over $[0, \mu_{\max}]$. The present approach is advantageous because $\mu(z)$ is nonlinear in z.

The recursion parameter sets for a subsonic boundary layer flow are summarized in table 1. The fast-stream values are denoted k_1 and $\bar{M}_{x,1}$, while the slow-stream values are denoted k_2 and $\bar{M}_{x,2}$. The acoustic modes must be computed for both the fast- and slow-stream values.

Type	Spacing	$\beta_+^{(j)}$	$\beta_-^{(j)}$
Vortical	$b^{(h)} = \frac{k_1}{\bar{M}_{x,1}} + \frac{h}{N_\omega}\left(\frac{k_2}{\bar{M}_{x,2}} - \frac{k_1}{\bar{M}_{x,1}}\right)$	$(1+i)b^{(j)}$	$\frac{-2k_2M_2}{1-M_2^2} - b^{(j)}$
	$h = 0, \ldots, N_\omega - 1$		
Evanescent acoustic	$\mu^{(h)} = \sqrt{k^2 - (1-\bar{M}_x^2)(\eta^{(h)})^2}$	$\frac{-\bar{M}_x k + \mu^{(j)}}{1-\bar{M}_x^2}$	$\frac{-\bar{M}_x k - \mu^{(j)}}{1-\bar{M}_x^2}$
	$h = 0, \ldots, N_e - 1$		
Propagating acoustic	$\theta^{(h)} = \frac{h}{N_p}\pi/2$	$k\frac{-\bar{M}_x + \cos\theta^{(2j)}}{1-\bar{M}_x^2}$	$k\frac{-\bar{M}_x - \cos\theta^{(2j+1)}}{1-\bar{M}_x^2}$
	$h = 0, \ldots, 2N_p - 1$		

Table 1 Recursion parameter sets for subsonic boundary layer flows.

Acknowledgments

This work has been supported by The Boeing Company through the Strategic Research and Development Relationship Agreement CT-BA-GTA-1.

References

[1] Smith, A., Company, D. A., Gamberoni, N., Sub-Committee, A. R. C. F. M., and Department, D. A. C. E. S. D. E., *Transition, Pressure Gradient and Stability Theory*, ARC-19322, Douglas Aircraft Company, El Segundo Division, 1956.

[2] Van Ingen, J., Sub-Committee, A. R. C. F. M., and Technische Hogeschool Delft, V., *A Suggested Semi-empirical Method for the Calculation of the Boundary Layer Transition Region*, ARC-19337, TH Delft, Delft, 1956.

[3] Crouch, J. D., and Ng, L. L., "Variable N-Factor Method for Transition Prediction in Three-Dimensional Boundary Layers," *AIAA Journal*, Vol. 38, No. 2, 2000, pp. 211–216. https://doi.org/10.2514/2.973.

[4] Fasel, H. F., Rist, U., and Konzelmann, U., "Numerical investigation of the three-dimensional development in boundary-layer transition," *AIAA Journal*, Vol. 28, No. 1, 1990, pp. 29–37. https://doi.org/10.2514/3.10349.

[5] Rist, U., and Fasel, H., "Direct numerical simulation of controlled transition in a flat-plate boundary layer," *Journal of Fluid Mechanics*, Vol. 298, 1995, p. 211–248. https://doi.org/10.1017/S0022112095003284.

[6] MA, Y., and ZHONG, X., "Receptivity of a supersonic boundary layer over a flat plate. Part 1. Wave structures and interactions," *Journal of Fluid Mechanics*, Vol. 488, 2003, p. 31–78. https://doi.org/10.1017/S0022112003004786.

[7] Bertolotti, F. P., Herbert, T., and Spalart, P. R., "Linear and nonlinear stability of the Blasius boundary layer," *Journal of Fluid Mechanics*, Vol. 242, 1992, p. 441–474. https://doi.org/10.1017/S0022112092002453.

[8] Day, M. J., "Structure and stability of compressible reacting mixing layers," Ph.D. thesis, Stanford University, California, Nov. 1999.

[9] Towne, A., Rigas, G., and Colonius, T., "A critical assessment of the parabolized stability equations," *Theoretical and Computational Fluid Dynamics*, Vol. 33, 2019. https://doi.org/10.1007/s00162-019-00498-8.

[10] Rigas, G., Colonius, T., and Beyar, M., "Stability of wall-bounded fows using one-way spatial integration of Navier-Stokes equations," *55th AIAA Aerospace Sciences Meeting*, 2017. https://doi.org/10.2514/6.2017-1881.

[11] Kamal, O., Rigas, G., Lakebrink, M. T., and Colonius, T., "Application of the One-Way Navier-Stokes (OWNS) Equations to Hypersonic Boundary Layers," *AIAA AVIATION 2020 FORUM*, 2020. https://doi.org/10.2514/6.2020-2986.

[12] Kamal, O., Rigas, G., Lakebrink, M., and Colonius, T., "Input/Output Analysis of Hypersonic Boundary Layers using the One-Way Navier-Stokes (OWNS) Equations," *AIAA AVIATION 2021 FORUM*, 2021. https://doi.org/10.2514/6.2021-2827.

[13] Kamal, O., Rigas, G., Lakebrink, M. T., and Colonius, T., "Input/output analysis of a Mach-6 cooled-wall hypersonic boundary layer using the One-Way Navier-Stokes (OWNS) Equations," *AIAA AVIATION 2022 Forum*, 2022. https://doi.org/10.2514/6.2022-3556.

[14] Towne, A., and Colonius, T., "One-way spatial integration of hyperbolic equations," *Journal of Computational Physics*, Vol. 300, 2015, pp. 844–861. https://doi.org/https://doi.org/10.1016/j.jcp.2015.08.015.

[15] Towne, A., Rigas, G., Kamal, O., Pickering, E., and Colonius, T., "Efficient global resolvent analysis via the one-way Navier–Stokes equations," *Journal of Fluid Mechanics*, Vol. 948, 2022, p. A9. https://doi.org/10.1017/jfm.2022.647.

[16] Kreiss, H.-O., "Initial boundary value problems for hyperbolic systems," *Communications on Pure and Applied Mathematics*, Vol. 23, No. 3, 1970, pp. 277–298. https://doi.org/https://doi.org/10.1002/cpa.3160230304.

[17] Thompson, K. W., "Time dependent boundary conditions for hyperbolic systems," *Journal of Computational Physics*, Vol. 68, No. 1, 1987, pp. 1–24. https://doi.org/https://doi.org/10.1016/0021-9991(87)90041-6, URL https://www.sciencedirect.com/science/article/pii/0021999187900416.

[18] Chang, C.-L., Malik, M. R., Erlebacher, G., and Hussaini, M. Y., "Linear and nonlinear PSE for compressible boundary layers," NASA Contractor Report 191537. Institute for Computer Applications in Science and Engineering (ICASE), September 1993.

[19] Zhu, M., and Towne, A., "Recursive one-way Navier-Stokes equations with PSE-like cost," *Journal of Computational Physics*, Vol. 473, 2023, p. 111744. https://doi.org/https://doi.org/10.1016/j.jcp.2022.111744, URL https://www.sciencedirect.com/science/article/pii/S0021999122008075.

[20] Joslin, R. D., Streett, C. L., and Chang, C. L., "Spatial direct numerical simulation of boundary-layer transition mechanisms: Validation of PSE theory," *Theoretical and Computational Fluid Dynamics*, Vol. 4, No. 6, 1993, pp. 271–288. https://doi.org/10.1007/BF00418777.